Research article

Aircraft turbine fan casing and ballistic fan blade impact: Geometry and material

Shade Rouxzeta VAN Der Merwe [a],[*], Dawood Ahmed Desai [b], Glen Campbell Snedden [c], Daniel Ogochukwu Okanigbe [d]

[a] Building 3, Office 314, Department of Mechanical Engineering and Mechatronics, Tshwane University of Technology, Main Campus, Pretoria West, Private bag X680 Staatsattilerie Road Pretoria 0001, South Africa
[b] Building 3, Office 307, Department of Mechanical Engineering and Mechatronics, Tshwane University of Technology, Main Campus, Pretoria West, Private bag X680 Staatsattilerie Road Pretoria 0001, South Africa
[c] Mechanical Engineering, Aerospace Systems Research Group, University of KwaZulu-Natal, Gate 3 Rick Turner Road, Glenwood, Durban, 4001, South Africa
[d] Pantheon Virtual Engineering Solutions, (PTY), Nigel,10 Apricot Avenue, Alra Park, 1491, South Africa

ARTICLE INFO

ABSTRACT

If the failed fan blade (FB) is not contained in the fan casing (FC) at the time of failure, a catastrophic disaster could follow from the failure of the aircraft's engine turbine. Unfavorable problems including the aircraft malfunctioning, a potential engine shutdown, and even a crash could occur if the detached FB enters the FC. This study employed the Finite Elements Method (FEM) to examine the effects of utilizing Polyether Ether Ketone (PEEK) as an alternative FB material on the FC in order to address this issue. In order to investigate the effects of PEEK and aluminum ballistic FB penetration on FC with thicknesses of 5, 4, 3, and 2 mm at 255 m/s, a FEM ballistic model was developed using the ABAQUS/Explicit modeling system. It was found that during working conditions, none of these FBs could pierce the FC, regardless of thickness. PEEK might be a better alternative, though, as the FC was more obviously deformed by the metal FB. The decision was made to conduct additional analytical validation of the developed FE models. The moment of inertia methodology, a novel approach, was employed. There was a strong correlation between the results of the FE models and the analytical answers. Therefore, it may be said that PEEK is a better material than aluminum for making blade casings.

1. Introduction

Somewhere in the world, a fan blade (FB) of an aircraft turbine engine will fail every few years [1–4]. If the engine FB of an airplane is not contained inside the fan casing (FC) when this failure happens, the unlikely but catastrophic outcome would happen. As a result, the aircraft's FC needs to be able to stop damage from a failed FB. An aircraft malfunction that puts the lives of the passengers at danger of death could result from the impact of an uncontained failed FB on an aircraft turbine engine. Therefore, it is critical to continue researching and improving the field of FB containment [1,5].

According to the literature that was available, a superior turbine FC structure to avoid failed FB penetration was obtained by

---

researching the behavior of various metallic materials and metal matrix composites. Additionally, these studies considered ways to reduce weight of the aircraft, which is essential for cost savings and for improved flight performance. For their investigations and assessments of FB confinement, the other researchers solely used metallic materials in the fan blades (FBs) they used. Therefore, their results confirmed the idea that the metallic FBs either penetrated the FC or result in a dent that has an impact on surrounding FBs and other parts both inside and outside the FC [6].

The containment of an FB that has failed from the rotor hub is reportedly one of the most difficult procedures in aviation engineering since it operates at high speeds and high energies, If the FB is not contained and fails or suffers secondary event damage, the proper operation of numerous engine components, such as the other FBs, the containment structure, surrounding fan casings (FCs), bearings, bearing supports, shafts, vanes, and externally mounted components, becomes compromised [7]. When a failed FB detaches from its hub and is not contained, such as when an aircraft malfunctions or an engine shuts down, it immediately causes secondary event damage. The majority of the time, the FB penetrates the FC, damaging the aircraft body structure. The containment structure, rotor, compressor, internal frames, inlet, and FC rub strips are all affected in various instances when the FB develops sharp edges and malfunctions [8].

Records going back decades have shown that secondary events brought on by uncontained engine failure, which has the unexpected effect of diminishing engine power, are the primary cause of the majority of aviation accidents. To prevent uncontained engine failure, numerous efforts must be made to develop dependable and efficient containment structures [9]. It is significant that there are no studies on polymer FBs in open-source literature. Studying the literature at hand revealed that no research has been done so far to examine the ballistic impact of a detached polymer FB on the turbine FC. A test would also be prohibitively expensive, hence it is important to perform an efficient computer analysis to mimic a polymer fan-blade out situation [10].

With the purpose of examining numerically the ballistic effect of a detached FB on its FC and the damage progression events that occur when the FB breaks, this study aims to investigate the utilization of metallic and non-metallic (polymer) FB materials. Investigations were done into the effects of changing the FC's dimension. The effect of aluminum and Polyether Ether Ketone (PEEK) FBs on a turbine FC with different thicknesses is evaluated in this study. The aviation sector may benefit from this study's recommendation of an alternate FB material for FB containment, which might increase aircraft safety and lighten weight.

2. Methodology

The methodology entails creating a quantitative numerical model to determine the FB's ballistic penetration on the FC. This was performed in ABAQUS/CAE 2017 by simulating a simple model design scenario for proprietary reasons and to make future experimental setup simple. The impacts that the two different FB materials (i.e. Aluminium and PEEK) received were taken into account when calculating the kinetic energy of each detached FB. Modeling the results of the FC being impacted by the two different FB materials was done using the Johnson-Cook damage approach. A recently created innovative methodology called the moment of inertia (MI) methodology was utilized to analytically validate the finite elements method (FEM) model [11]. Map forward: Mathematical modeling, Numerical Modelling, Analytical validation technique: moment of inertia methodology.

This study did not consider the following: aerospace atmospheric forces, the fatigue failure of the blade, coriolis and gyroscopic forces (These forces are critical for consideration only when the blade is attached to the rotor hub and such a scenario was not considered in this study), the vibration of the rotor, casing or other blades and simulating destruction processes.

2.1. Mathematical modeling

In order to investigate the ballistic impact of the released blade on the engine casing, relevant mathematical models were used to characterize the transient dynamic behavior of the FB. This includes the FB Impact Velocity, Impact energies and stresses on the engine
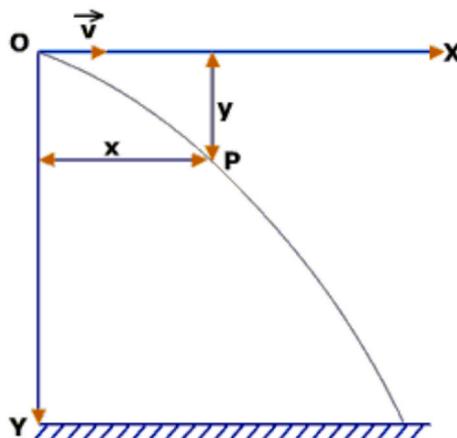
Fig. 1. Horizontal projectile's trajectory [12].

casing, Failure Modes of the released FB, Critical Velocity for Plate Perforation, Johnson-Cook Damage Model.

2.1.1. FB impact velocity

The study made the premise that the FB's trajectory is linear because of the small amount of distance (i.e. 1 mm) over which an FB travels. Fig. 1 depicts the FB that has been separated moving as expected.

x is ignored in this analysis due to the FB projectile's (i.e. 1 mm) short distance before hitting the FC. Eqs. (1)–(3)'s descriptions of Newton's laws were used to calculate the ballistic trajectory impact [13]. In Eqn (1): N represents its rotational speed and ω its angular velocity. Eq. (2) depicts the turbine's linear velocity in which initial linear velocity of the FB is taken to be zero, while V_f is the final linear velocity and r_{b1} is the distance from the hub turbine's center to the outer half of the FB. The projectile time t can be defined as the time it takes for the detached FB to touch the FC. x is the tip clearance or distance traveled by the detached FB (from launch to impact on the FC).

$$\omega = \frac{\pi}{60}N \tag{1}$$

$$V_f = \omega . r_{b1} \tag{2}$$

$$t = \frac{x}{V_f} \tag{3}$$

The projectile time t was computed using the following values: N = 32 500 r/min, r_{b1} = 0.075 mm, and x = 1 mm are given by the council for scientific and industrial research (CSIR) [12]. The outcome is that the numerical simulation modeling will start up in 3.99 X 10^{-6} s.

$$V_f = \frac{2\pi \, X \, 32500}{60} \, X \, 0.075$$

$$= 255.25 \text{ m/s}$$

$$t = \frac{0.001 \, m}{255.25 \, m/s}$$

$$= 3.99 \, X \, 10^{-6} \, s$$

2.1.2. Impact energies and stresses on the engine casing

A sensitivity analysis was conducted in this work, which examined various FB materials and FC thickness changes. The mass and speed of the separated FB, as given in Eq. (4), define the impact energy:

$$K = \frac{1}{2}mV_f^2 \tag{4}$$

Where m is the mass of the FBs, K is the total kinetic energy prior to impact, and V_f is the previously determined linear impact velocity (Eq. (2)). Kinetic energy is the primary factor in fragmentation [14]. In this work, two different ductile materials—aluminum and PEEK—are looked into as viable FB materials. The highest bending forces and deflection at the site of impact were thus the study's focus points. Fig. 2 depicts a schematic of the actual FB and FC configuration. According to Sharma et al.'s [15] research of this impact issue, shape change or dimensional instability is the factor that influences penetration. Hence, the focus of the study for the bending
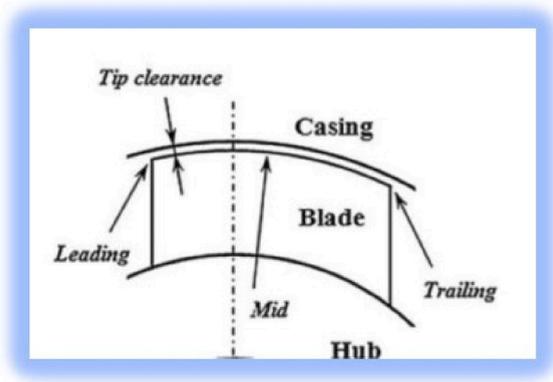
Fig. 2. FB and FC schematic [12].

axis was the center axis.

The MI, which was the main variable used to calculate the impact stress, deflection, and strain energy, is described by the relationship stated mathematically (Eq. (5)). I represents the Moment of Inertia in Equation (5), along with the letters b for the FBs breath and h for the FC plate's thickness.

$$I = \frac{bh^3}{12} \tag{5}$$

I represents the Moment of Inertia in Equation (5), along with the letters b for the FBs breath and h for the FC plate's thickness. Eq. (6) establishes the static stress at the FC's point of impact, according to Moon et al. [16]. Where t denotes the impact simulation time, F denotes the impact force, L denotes the FC's length, and s denotes the static stress impact at the center. The appropriate FC plate thickness was determined using the maximum deflection of FC after contact based on Eq. (7) [13,16]. The maximum stress placed on the FC after impact was determined using Eq. (8) (Moon et al. [16]). Eq. (9) [7] is used to determine how much energy the FC stored due to deformation after impacted. Eq. (10) is used to determine the moment (M).The force of the FB's impact on the FC is determined with Eq. (11), where FBs mass and acceleration are denoted by m and a, respectively.

$$\sigma_s = \frac{Fl^2\, t}{8I} \tag{6}$$

$$d = \frac{Fl^3}{192EI} \tag{7}$$

$$\sigma_{max} = \left[1 + \left(1 + \frac{2hE}{L\sigma_s} \right)^{0.5} \right] \tag{8}$$

$$U = \frac{M^2}{2EI} \tag{9}$$

$$M = \frac{FL}{8} \tag{10}$$

$$F = ma \tag{11}$$

2.1.3. Failure Modes of the released FB

The detached FB is released with a specific kinetic energy when the stress surpasses the ultimate tensile strength of the FB material [14,17]. In this investigation, it was assumed that the FB material was ductile and that it would plug when the critical impact velocity was reached [18].

2.1.4. Critical Velocity for Plate Perforation

The speed at which the FB pierces the FC with great force is known as the critical projectile velocity [19] and is represented mathematically by Eq. (12). V_x is the minimum perforation velocity and m_p is the plug mass.

$$V_c^2 = \left[\frac{m}{m + m_p} \right] \left(V_f^2 + V_x^2 \right)^{0.5} \tag{12}$$

2.1.5. Johnson-Cook Damage Model

Impact research is best solved by the Johnson-Cook (J-C) model, which has the benefit of being able to distinguish between the three essential elements of stress, strain hardening, and temperature [20]. Furthermore, for assessments of the current issue, the Johnson-Cook model was selected as a more suitable damage model [21]. There is a stress threshold for each material that determines when it will completely fail or keep withstanding loads without leading to a corresponding rise in strain [22]. The model is suitable to evaluate FB confinement research and has been shown experimentally to be viable for strain rates up to and about 104 s^{-1} [21]. For this analysis, a strain rate of 102 s^{-1} was used, which is within the allowed range [21]. The J-C model is expressed in Eq. (13) and σ_e is the von Mises flow stress, A, B, C, n and m are considered to be material constants and ε^p is the equivalent plastic strain given in Eq. (14). Where $\varepsilon*$ is the dimensionless strain rate and $\varepsilon_0 = 1s^1$. The homologous temperature $T*$ is expressed in Eq. (15). T is the absolute temperature, T_o is the room temperature, and T_m is the melting temperature of the material. T temperature rises at the plastic work region; the heat produced by plastic work at the impact zone is considered to be adiabatic and is stated in Eq. (18) [23]. The J-C damage model is conditioned by damage evolution. The damage D of a material is expressed in Eq. (16). The fracture strain εf is expressed in Eq. (17). β is the fraction of plastic work converted, σ_s bending stress and σ contact stress.

$$\sigma_e = \left[A + B\left(\varepsilon^P \right)^n \right] \left[1 + Clin\dot{\varepsilon}^* \right] \left[1 - T^{*m} \right] \tag{13}$$

$$\dot{\varepsilon}^* \frac{\varepsilon^p}{\varepsilon_0} \tag{14}$$

$$T^* = \frac{T - T_o}{T_m - T_o} \tag{15}$$

$$D = \sum \frac{\Delta \varepsilon^p}{\varepsilon_f} \tag{16}$$

$$\varepsilon_f = \left(D_1 + D_2 e^{D_3 \sigma^*}\right)\left(1 + D_4 lin\ \dot{\varepsilon}^*\right)\left(1 + D_5 T^*\right) \tag{17}$$

$$T = \int \frac{\beta}{\sigma_s} \sigma\ \Bigg(\tag{18}$$

2.2. Numerical Modelling

The strategies and design techniques used to model the impact interaction between the different materials under evaluation and the FB confinement are described in detail, along with the steps taken to create the finite element analysis (FEA) and the method by which the FB and FC were simulated in order to develop the appropriate analytical input files.

2.2.1. Model development

To simplify the FB model, a rectangular shape with the following dimensions was used: 22 mm for width, 37 mm for length, and 2 mm for thickness (Fig. 3). The dimensions of a small aircraft engine utilized in the industry were used to build the FB containment assembly. The ABAQUS CAE 2017 FEA program was used to construct the model.

2.2.2. Material properties

PEEK 1000 and aluminum 6082-T651 were selected as the FB materials in this study, whereas aluminum 6082-T651 was selected as the FC material [24]. For this experiment, the materials were deemed to be homogeneous and isotropic. The material properties for PEEK (Garcia-Gonzalez, Rusinek, Jankowiak, and Arias [26]) and aluminum (Boldyrev, Shchurov, and Nikonov [25]) are displayed in Table 1 through 4. According to He et al. [27], the J-C constitutive relation is a suitable method for this specific engineering problem, especially when there are many FB materials and different FC thicknesses. Tables 2 and 3 display the J-C constants and damage constants for PEEK and aluminum, respectively. It is assumed that the high velocity impact of the FB onto the FC is adiabatic because the heat generated by the plastic work at the impact location does not have enough time to be transferred to the surrounding material. Table 4 lists the adiabatic properties of PEEK and aluminum. Aerodynamic forces were thought to have little effect on the analysis, but it was found that the aircraft turbine could operate up to 32 500 feet, or 9.75 km, above the ground [24].

2.2.3. Assembly module

The assembly module is controlled by the formulas. In this step, the various parts that were generated are combined into a single unit. In the assembly module, the components are put together at certain locations. The location of the FB within the assembly affects the analysis. The FB was thus placed in the center of the FC. An inappropriately positioned FB in the assembly will immediately change the simulation results by increasing the discrepancy between numerical and analytical results. Boundary conditions and interactions, including planned loading and interactions, are impacted by the assembly. In the real aircraft turbine engine design, a 1 mm gap is permitted between the FB and FC. Consequently, the FB was shifted to the center of the FC with a design clearance of 1 mm, and the FC was fixed for the analysis in this study. This is depicted in Fig. 4.
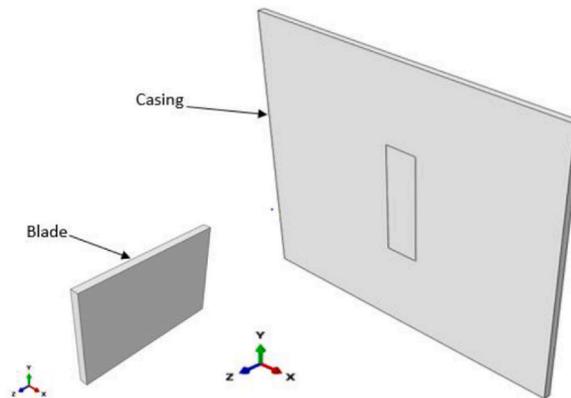
Fig. 3. Segment of the FB and FC in geometric form.

Table 1

Mechanical material properties of Aluminium and PEEK [25,26].

Property	Units	Aluminium	PEEK
Elastic Modulus (E)	GPa	70	3.6
Density (ρ)	kg/m^3	2700	1304
Poisson's ratio(v)		0.33	0.4
Kinetic Friction coefficient (μ)		1.4	1

Table 2

J-C constants of Aluminium and PEEK [25,26].

Property	Units	Aluminium	PEEK
Yield strength (A)	MPa	324.1	132
Hardening coefficient (B)	MPa	113.8	10
Strain hardening exponent (n)		0.42	1.2
Strain rate constant (C)		0.0074	0.034
Softening exponent (m)		1.4	0.7
Melting temperature (Tm)	K	855	614

Table 3

Damage constants of Aluminium and PEEK [25,26].

Property	Aluminium	PEEK
Damage constant (D_1)	−0.77	0.05
Damage constant (D_2)	1.45	1.2
Damage constant (D_3)	−0.47	−0.254
Damage constant (D_4)	0	0
Damage constant (D_5)	1.6	1

Table 4

Adiabatic properties of Aluminium and PEEK [25,26].

Property	Units	Aluminium	PEEK
Specific heat (Cp)	J/kgk	923	2180
Inelastic		0.9	0.9
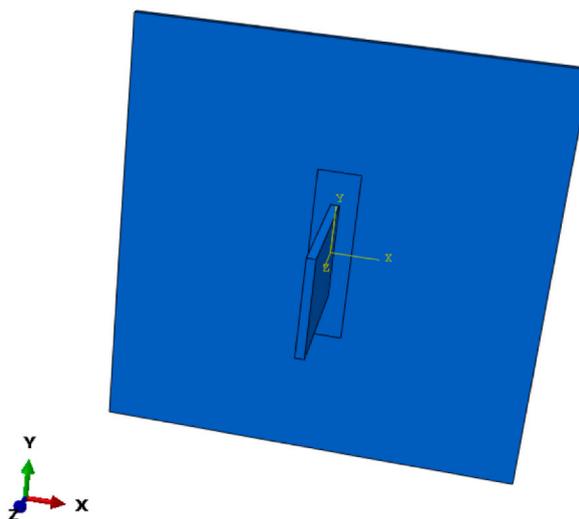
Fig. 4. Assembled model.

2.2.4. Step module

The sequence in which analyses of the generated model were carried out is displayed in the two sections of the step module. According to the ABAQUS default setup, the first step is defined first. This step defines all relevant beginning conditions, such as loads, interactions, boundary conditions, and predefined fields. The second stage that is developed is the dynamic explicit phase, which is intended to mimic the effect of the FB against the FC. The minimum time interval for the dynamic step is set at 0.002 s since this is thought to be appropriate for the study and gives enough time to determine if the FB will pierce or just bounce off. The output variables employed for this inquiry are the strain energy, the kinetic energy, and the stress in the z direction, which contributed to the model's deformation. The interactions between FB and FC are influenced by each of these factors [28] "Interaction" refers to the relationship between the surfaces, e.g., the contact between the FB and FC. Because it is the only method capable of capturing high impact deformation during short time dynamic evaluations, an explicit contact interaction strategy was selected for this investigation. Throughout the analysis, there is hard contact mechanical behavior because of the tremendous force with which the FB contacts the FC. It is anticipated that when the FB hits the FC, friction will cause the surfaces it creates to become heated.

2.2.5. Mesh generation

Since mesh generation influences the FE model's computation time and result correctness, it is an essential part of simulation. The more simulation parts there are, the more processing power is needed to do the study. Since local meshing accelerates computation, it is believed to be more advantageous to split the component at the location of interest and use it for other portions. Mesh controls were used to define the element's dimensions. Mesh refinement was carried out in the partitioned section (the place of interest) on the FC in order to obtain more accurate results. The divided area on the FC is seen in Fig. 5 of the completed model. This work used a dynamic explicit analysis, hence a suitable mesh was needed to accurately represent the FB impact. The selection of hexahedral element types was based on their improved convergence, lower computational cost and time, and increased precision compared to tetrahedral elements [29]. Following the guidelines and standards provided by the software, three-dimensional eight-node hexahedral elements of type C3D8I were the main elements used. Default hourglass controls were specified in order to prevent shear locking, which could result in fake solutions [30]. Table 5 shows the number of nodes and components in the model for each of the possible scenarios. Because to FB's tremendous impact, significant deformation and associated elemental distortion are expected at the impact zone. Consequently, adaptive meshing was selected to yield accurate results and a mesh. A mesh quality check was done to evaluate the nodes' stability. As illustrated in Fig. 5, mesh refinement was applied to the partitioned portion.

2.2.6. Mesh convergence study

In order to shorten calculation times and generate findings that are sufficient and precise, a mesh convergence research is carried out [31]. The mesh seed size is halved after every analysis to increase the number of elements until convergence is achieved. Table 6 above displays the mesh convergence study for the 5 mm and 4 mm FC thickness, and Table 7 displays the mesh convergence study for
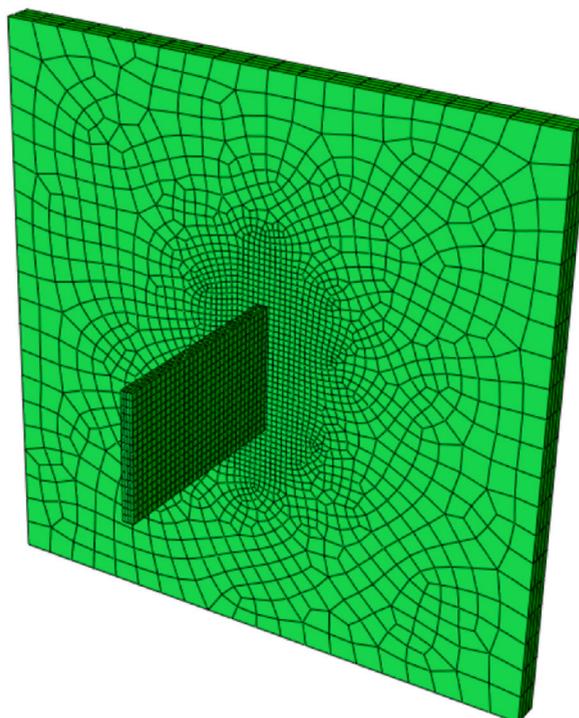
Fig. 5. Mesh refinement on the whole model: FB and FC.

Table 5
Number of nodes and elements of the model in different FC.

FC thickness (mm)	Number of nodes	Number of elements
2	5442	5406
3	7612	7668
4	10 584	13 576
5	13 781	10 506

the 3 mm and 2 mm FC thickness. Reducing the seed size resulted in a finer mesh that had a higher element density. The mesh convergence analysis presented in Table 6 led to the conclusion that the optimum seed size was 1 mm, since this resulted in results with an impact stress deviation of less than 10 % and a deflection deviation of 5 %. Consequently, a mesh size of 1 mm was selected for this investigation. Based on the mesh convergence study shown in Tables 7 and it was determined that the seed size of 1 mm was dependable when the deflection and impact percentage errors were both less than 10 %. As a result, a 1 mm mesh size was selected.

2.2.7. Boundary conditions

In order to imitate the FB containment's operational restrictions, the model's boundary conditions were set. The model was given displacement and rotation as boundary conditions [28]. There are not many restrictions at the entry and exit of the FC, which is essentially cylindrical. Since the impact happens at a specific location (the section under investigation), the boundary conditions in this study were predicated on the existence of a beam-like restriction. The following restrictions apply to the simplified FC in Fig. 6. Since the impact takes place in the center of the FC, which is split into four equal sections, it was expected that the left and right sides would be fixed in a manner akin to a building beam. As a result, the rotation in the x, y, and z axes as well as the displacements on the left and right sides of the FC are equal to zero. The top and bottom of the FC were permitted to distort as a result of the impact load produced by the FB. As illustrated in Fig. 6, the FC's top and bottom were only allowed to deform in the z-direction and were not allowed to move or rotate in the x- or y-directions, respectively. The boundary conditions are unrestricted because it is assumed that the FB and hub have been split apart.

2.2.8. Predefined field

The preset field dictates the kind of analysis the model conducts. Aerodynamic forces were assumed to have no effect on the FB confinement. However, adiabatic effects were considered because the objective of this analysis was to determine the FC's deformation features that were impacted by different FB materials [8]. The velocity in the z-direction, which was fixed at 255 m/s, was obtained using Eq. (2). Jamison, Snedden, and Turner [24] reported that as a result, the FB struck the FC at a speed of 255 m/s. Table 8 displays the cases this study looked at.

2.3. Definition of outputs

2.3.1. Field outputs

The field outputs that were needed for this analysis were the components of stress, displacement, strain, and contact forces and responses.

2.3.2. History outputs

The history outcomes of kinetic energy, strain energy, plastic dissipation, and damage dissipation were selected for this study. Fig. 7 provides an overview of the approach utilized in the numerical model's development and analysis.

2.4. Analytical validation technique: the moment of inertia methodology

Forward map: developed analytical validation technique, the assumptions for the development of the MI methodology.

2.4.1. Developed analytical validation technique

As alluded to earlier, the MI methodology was created to validate the formulated numerical model. Utilizing the newly developed MI approach, the stress, deflection, and strain energy of the eight modeling case scenarios—FC thicknesses of 5, 4, 3, and 2 mm struck by FBs made of aluminum 6082-T651 and PEEK 1000—were validated. Inertia of the swing of a baseball bat was examined by Koenig et al. [32] and their research showed that when swinging a bat to hit a baseball to score, the MI and the mass of the bat are two

Table 6
Mesh convergence study on 5 mm and 4 mm FC.

Mesh size (mm)	Stress (MPa)	Deflection (mm)	Percentage error for stress (%)	Percentage error for deflection (%)
2	18.23	0.535	7	7
1	20.8	0.548	8	5
0.5	19	0.636	14	5

Table 7

Mesh convergence study on 3 mm and 2 mm FC.

Mesh size (mm)	Stress (MPa)	Deflection (mm)	Percentage difference for stress (%)	Percentage difference for deflection (%)
2	218	5.481	30	11
1	160	5.216	5	9
0.5	102	5.419	45	14
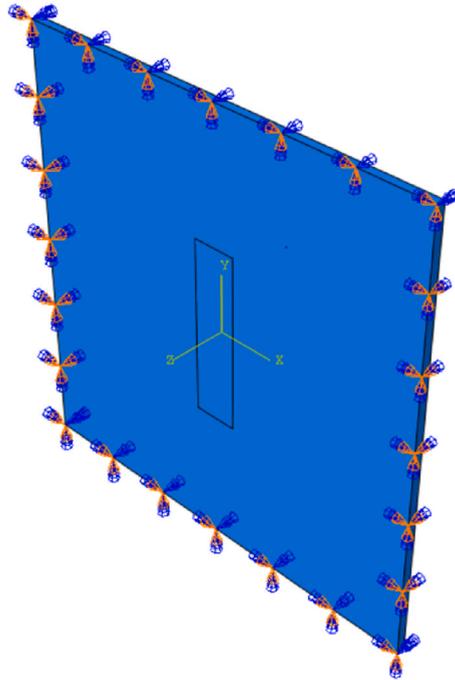
Fig. 6. Boundary conditions.

Table 8

Case scenarios and descriptions.

Case scenarios	Description
1	5 mm FC and aluminium FB
2	5 mm FC and PEEK FB
3	4 mm FC and aluminium FB
4	4 mm FC and PEEK FB
5	3 mm FC and aluminium FB
6	3 mm FC and PEEK FB
7	2 mm FC and aluminium FB
8	2 mm FC and PEEK FB

important factors to consider. Sharma et al. [15] studied the ballistic impact of three different metals with a target-to-projectile thickness ratio of 1:0.5. They noticed that none of the metal bullets penetrated the plate target below a speed of 700 m/s, but that when the projectile hit the plate, it bulged and took on a different shape. The MI methodology was created using the combined approaches of Sharma et al. [15] and Koenig et al. [32]. In this study, FC to FB ratios of 2.5:1, 2:1, 1.5:1, and 1:1 were considered. The projectile's change in shape was also taken into account. According to the experiments in the Sharma et al. [15] study, the sphere projectile's diameter rose from 10 mm to 14 mm after impact.

2.4.2. The assumptions for the development of the MI methodology

The following are the assumptions used to establish the moment of inertia methodology.

- The projectile's mass and material properties would remain unchanged after the collision, only its MI would be affected by its altered shape.
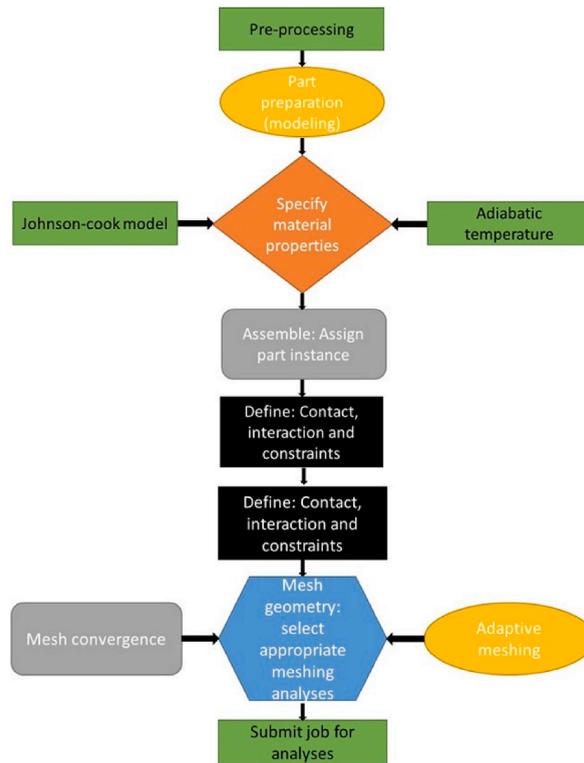
Fig. 7. overview of the approach utilized in the numerical model's development and analysis.

- The rectangular projectile's width would decrease after impact or impact the casing at various increments of the FB width during impact.
- The projectile's MI would vary with each increment of form change.
- It was assumed that the surface of the projectile that makes contact with the target changes shape, and that the impact zone of the target would deform in the shape of the projectile, implying that the thickness of the target is a key factor in the change of the MI.

The focus of this study's investigation on the FC (which came in a variety of thicknesses) was the breadth of the FB. The MI was used as the mean variable to determine the deflection, maximum stress, and strain energy at the point of impact. The FB impacts the FC at a linear speed of 255 m/s (as the distance considered is very short, i.e. 1 mm). Modeled as a straightforward rectangle plate with measurements of 32 mm by 22 mm by 2 mm, the FC was square in shape and was 100 mm by 100 mm. Although the mass and speed remained constant, the computer model showed that the FB bulges after impact, changing its shape. Indicating a phenomenon of change at the MI during contact on the FC, the FC took on the shape of the FB at the point of impact. As shown in Fig. 8, the blade's shape changes the breadth or height after impact, which changes the magnitude of the MI for the FC. Eq. (5) can be used to calculate
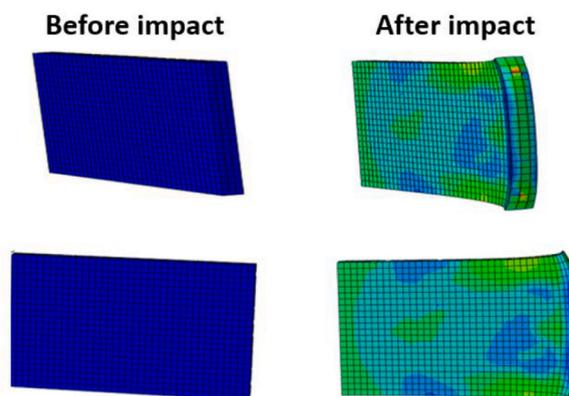
Fig. 8. the FB shape before impacting FC (left) and the FB shape after impacting FC (right).

the MI. The impact force of the FB on the FC is proportional to the width of the FB. Since the blade's shape changes, this analysis assumes that just its breadth does, with all other factors remaining unchanged.

2.4.3. Illustration and validation of simulations using the MI methodology

In this investigation, the impact FB's original width is taken and decreased from 22 mm to 1 mm by 1 mm. The height variable in Eq. (5) denotes the thickness of the FC, which ranged from 5 mm to 2 mm. The MI in m^4 for various FC thicknesses and widths is shown in Table 9.

Since all other variables depend on the MI, they could all be estimated after the MI in each range was determined. For L = 100 mm, t = 0.002 s, Eq. (6) was used to compute the stress on the FC. Eq. (10) yields the force F, where F for the aluminum FB was measured at 785.4 N and F for PEEK at 280.5 N. Tables 10 and 11 give the stress from impacts with FBs made of aluminum and PEEK, respectively.

From Eq. (7), we can calculate the deflection of the FC following impact. The predicted deflection on the FC caused by the impact of aluminum and PEEK FC is shown in Tables 12 and 13, respectively.

Tables 14 and 15, which show the strain energy on the FC affected by an aluminum FB and a PEEK FB, respectively, show the results of calculating the strain energy of the FC after impact using Eq. (8).

3. Results

3.1. Validation of simulations using the MI methodology

The simulation results that were verified by the MI approach are presented. Analysis was done on the deflection, maximum stress, and strain energy as well as the effects of the aluminum and PEEK FB impacting the aluminum FC. The FC under consideration ranged in thickness from 5 mm to 4 mm–3 mm to 2 mm. The study's main focus was on the effect the FB has on the FC after impact because they are thrown away after the incident. It was determined that the damage to the FC was limited to a dent and that no penetration had occurred. The degree of the FC's deformation revealed the recommended FC thickness for use in the final FC designs. As a result, the advice was given in an effort to prevent any secondary damaging consequences, such as compressed or damaged wires and sensors, which could lead to an aircraft malfunction. Where the FB would penetrate the FC is indicated, by the maximum stress. Eq. (13) was used to compute the maximum stress. MI were used for all calculations. The number of elements along the border of the FC thickness and the size of the components in the impact zone have a significant impact on the outcome and the relationship between the simulation and the MI methodology.

3.1.1. Stress and deflection

8 cases were investigated and the results are demonstrated in a sensitivity analysis style. 2 case scenarios of the 8 cases is demonstrated explicitly, due to the paper's maximum size. The simulation's 3D visualization results, which display deflection following impact, are shown in Figs. 9–12. Additionally, they display the maximum stress dissipation of the FC when it is impacted by an aluminum or PEEK FB at 1 and 2 ms, respectively; these represent case scenario 1 and case scenario 2. The numbers in Tables 16 and 17 were calculated using the MI methodology.

Table 9
The MI (m^4) for the different thicknesses and different breadths.

Breadth (mm)	MI (m^4) for different casing thicknesses			
	5 mm	4 mm	3 mm	2 mm
22	2.3×10^{-10}	1.2×10^{-10}	4.9×10^{-11}	1.5×10^{-11}
21	2.2×10^{-10}	1.1×10^{-10}	4.7×10^{-11}	1.4×10^{-11}
20	2.1×10^{-10}	1.1×10^{-10}	4.7×10^{-11}	1.3×10^{-11}
19	1.9×10^{-10}	1×10^{-10}	4.3×10^{-11}	1.3×10^{-11}
18	1.8×10^{-10}	9.6×10^{-11}	4×10^{-11}	1.2×10^{-11}
17	1.7×10^{-10}	9.1×10^{-11}	3.8×10^{-11}	1.1×10^{-11}
16	1.6×10^{-10}	8.5×10^{-11}	3.6×10^{-11}	1×10^{-11}
15	1.5×10^{-10}	8×10^{-11}	3.4×10^{-11}	1×10^{-11}
14	1.4×10^{-10}	7.5×10^{-11}	3.2×10^{-11}	9.4×10^{-12}
13	1.3×10^{-10}	6.9×10^{-11}	3×10^{-11}	8.7×10^{-12}
12	1.1×10^{-10}	6.4×10^{-11}	2.7×10^{-11}	8×10^{-12}
11	1×10^{-10}	5.9×10^{-11}	2.5×10^{-11}	7.3×10^{-12}
10	1×10^{-10}	5.3×10^{-11}	2.3×10^{-11}	6.7×10^{-12}
9	9.4×10^{-11}	4.8×10^{-11}	2×10^{-11}	6×10^{-12}
8	8×10^{-11}	4.3×10^{-11}	1.8×10^{-11}	5.3×10^{-12}
7	7×10^{-11}	3.7×10^{-11}	1.6×10^{-11}	4.7×10^{-12}
6	6×10^{-11}	3.2×10^{-11}	4×10^{-11}	4×10^{-12}
5	5×10^{-11}	2.7×10^{-11}	1.1×10^{-11}	3.3×10^{-12}
4	4×10^{-11}	2.1×10^{-11}	9.4×10^{-12}	2.7×10^{-12}
3	3×10^{-11}	1.6×10^{-11}	6.7×10^{-12}	2×10^{-12}
2	2×10^{-11}	1.1×10^{-11}	4.5×10^{-12}	1.3×10^{-12}
1	1×10^{-11}	5.3×10^{-12}	2.3×10^{-12}	6.7×10^{-13}

Table 10
Stress on FC caused by Aluminium FB impact.

Breadth (mm)	MI (m^4) for different FC thicknesses			
	5 mm	4 mm	3 mm	2 mm
22	9.1	17	40	134
21	9.5	18	42	140
20	9.8	18	44	147
19	10	19	46	155
18	12	20	48	164
17	13	22	51	173
16	14	23	55	184
15	15	25	58	196
14	17	26	62	210
13	18	28	67	227
12	20	31	73	245
11	21	33	79	268
10	22	37	87	295
9	25	41	97	327
8	28	46	110	368
7	30	53	120	421
6	30	61	150	491
5	40	74	170	589
4	50	92	220	736
3	60	120	290	982
2	90	180	440	1470
1	200	370	870	2950

Table 11
Stress on FC caused by PEEK FB impact.

Breadth (mm)	MI (m^4) for different FC thicknesses			
	5 mm	4 mm	3 mm	2 mm
22	3	6	14	48
21	3.2	6	15	50
20	3.5	7	16	53
19	4	7	16	55
18	4	7.3	17	58
17	4.1	8	18	62
16	4.2	8	19	66
15	4.8	9	21	70
14	5	9	22	75
13	5	10	24	81
12	6	11	26	88
11	6	12	28	96
10	7	15	31	110
9	7	16	35	120
8	8	20	39	130
7	10	20	45	150
6	10	23	52	180
5	11	30	62	210
4	20	30	78	260
3	20	40	100	350
2	30	70	160	530
1	70	100	310	1100

3.2. Case scenario 1

Case scenario 1 shows the impact of an aluminum FB on a 5 mm thick FC. The simulated deflection in Fig. 9 was 1.01 mm. The dimensional instability is shown in Table 16 to occur at a breadth of 5 mm, a MI of 5.2×10^{-11} m^4, and a deflection of 1.11 mm. This showed a 9 % difference in percentage between the analytical results and the simulated results. According to Table 16, the static stress on the FC at 5.2×10^{-11} m^4 of MI is 40 MPa. The maximum stress upon impact (280 MPa), was calculated using Eq. (14) with the static stress value of 40 MPa. The analytically estimated stress was 280 MPa and the maximum stress of the simulation in Fig. 10 was 288.7 MPa, resulting in a 3 % inaccuracy.

Table 12
Deflection of FC impacted with an Aluminium FB.

Breadth (mm)	MI (m⁴) for different FC thicknesses			
	5 mm	4 mm	3 mm	2 mm
22	0.255	0.498	1.18	3.98
21	0.267	0.522	1.24	4.17
20	0.281	0.548	1.3	4.38
19	0.295	0.577	1.37	4.61
18	0.312	0.609	1.44	4.87
17	0.33	0.645	1.53	5.16
16	0.351	0.685	1.62	5.48
15	0.374	0.703	1.73	5.84
14	0.401	0.783	1.86	6.26
13	0.432	0.843	2	6.74
12	0.468	0.9137	2.16	7.3
11	0.51	0.996	2.36	7.97
10	0.561	1.1	2.6	8.77
9	0.623	1.22	2.89	9.74
8	0.701	1.37	3.25	11
7	0.801	1.57	3.71	12.5
6	0.935	1.83	4.33	14.6
5	1.12	2.19	5.19	17.5
4	1.4	2.74	6.49	21.9
3	1.87	3.65	8.66	29.1
2	2.8	5.48	13	43.8
1	5.61	11	26	87.7

Table 13
Deflection of FC impacted with a PEEK FB.

Breadth (mm)	MI (m⁴) for different FC thicknesses			
	5 mm	4 mm	3 mm	2 mm
22	0.0911	0.178	0.422	1.42
21	0.0977	0.186	0.442	1.49
20	0.01	0.196	0.464	1.57
19	0.0105	0.206	0.488	1.67
18	0.011	0.217	0.4	1.74
17	0.0111	0.23	0.546	1.84
16	0.0125	0.245	0.58	1.96
15	0.0134	0.261	0.618	2.09
14	0.0143	0.28	0.663	2.24
13	0.0154	0.301	0.714	2.41
12	0.0167	0.326	0.773	2.61
11	0.0182	0.356	0.843	2.85
10	0.02	0.391	0.928	3.13
9	0.0223	0.435	1.03	3.48
8	0.025	0.489	1.16	3.91
7	0.0286	0.559	1.33	4.47
6	0.0334	0.652	1.55	5.22
5	0.0401	0.783	1.86	6.26
4	0.0501	0.978	2.32	7.83
3	0.0668	1.3	3.09	10.4
2	1	1.96	4.64	15.7
1	2	3.9	9.28	31.3

3.3. Case scenario 2

Case 2 shows the impact of a PEEK FB on a 5 mm thick FC. Fig. 11. It shows that the simulation deflection was 0.41 mm, but Table 17 demonstrates that at the breadth of 5 mm, the dimensional instability occurs and determines the MI of 5.2 x 10⁻¹¹ m⁴, while the deflection was 0.401 mm, giving an error margin of about 2 % between the simulation and analytical results. Similarly, the maximum stress of 148 MPa was calculated using the static stress of 13 MPa found in Table 17. After impact, the simulation's highest stress was 137 MPa, which was 7 % higher than the theoretically predicted stress (See Fig. 12). A decrease in tension was seen as it approached the support end. This is explained by the force and resistance of the FC at the impact location being rather insignificant.

3.3.1. Strain energy graphs

The graphical details of the simulation and analytical strain energy for case scenarios 1 and 2 are shown in Figs. 13 and 14,

Table 14

Strain energy of FC impacted with an aluminium FB.

Breadth (mm)	MI (m^4) for different FC thicknesses			
	5 mm	4 mm	3 mm	2 mm
22	1.53	2.99	2.1	2.39
21	1.61	3.14	2.43	2.51
20	1.69	3.29	2.81	2.63
19	1.77	3.47	8.22	2.77
18	1.87	3.66	8.67	2.93
17	1.98	3.87	9.18	3.1
16	2.11	4.12	9.76	3.29
15	2.25	4.39	10.4	3.51
14	2.41	4.7	11.2	3.76
13	2.59	5.07	12	4.09
12	2.81	5.49	13	4.39
11	3.07	5.99	14	4.79
10	3.37	6.59	15.6	5.27
9	3.75	7.32	17.3	5.85
8	4.22	8.23	19.5	6.59
7	4.82	9.41	22.3	7.53
6	5.62	11	26	8.78
5	6.74	13.2	31.2	10.5
4	8.43	16.5	39	13.2
3	11.3	22	52	17.6
2	16.9	32.9.	78.1	26.3
1	33.1	69	156	52.2

Table 15

Strain energy of FC impacted with a PEEK FB.

Breadth (mm)	MI (m^4) for different FC thicknesses			
	5 mm	4 mm	3 mm	2 mm
22	0.345	0.697	1.65	0.557
21	0.375	0.73	1.73	0.584
20	0.392	0.766	1.82	0.613
19	0.431	0.806	1.91	0.645
18	0.436	0.851	2.02	0.681
17	0.461	0.901	2.14	0.721
16	0.49	0.958	2.27	0.766
15	0.523	1.02	2.42	0.871
14	0.56	1.09	2.59	0.876
13	0.603	1.18	2.79	0.94
12	0.654	1.28	3.03	1.02
11	0.713	1.39	3.3	1.11
10	0.785	1.53	3.63	1.23
9	0.872	1.75	4.04	1.36
8	0.981	1.93	4.54	1.53
7	1.12	2.19	5.19	1.75
6	1.31	2.55	6.05	2.04
5	1.57	3.06	7.26	2.45
4	1.96	3.83	9.08	3.06
3	7.85	5.11	12.1	4.09
2	35.7	7.66	18	6.13
1	37.4	15.1	36.3	12.3

By reducing the breadth and FC thickness (which reflects the height), the MI methodology's study has been shown. The numerical model assessed the following section of this methodology.

respectively. The graphs show the same flow of dynamic penetration effects over time for both the simulation and the analytical calculations, with case scenario 1's dynamic impact effect becoming more stable and case scenario 2's dynamic impact effect becoming unstable due to polymer bounce effects on impact. At the point of impact, the strain energy was at its highest; over time, the energy decreases. Due to the impact force being higher than that of PEEK FB, FC impact with aluminum FB stores more energy.

3.3.2. Kinetic energy

The kinetic energy behavior of the PEEK and aluminum FB is shown in Fig. 15. According to the image, the PEEK FB had a lower pitch of kinetic energy than the aluminum FB. Therefore, it is obvious that the FC has suffered more deformation as a result of the aluminum FB. The kinetic energy pitch of the PEEK and aluminum FBs persisted for 0.3 ms before stabilizing.
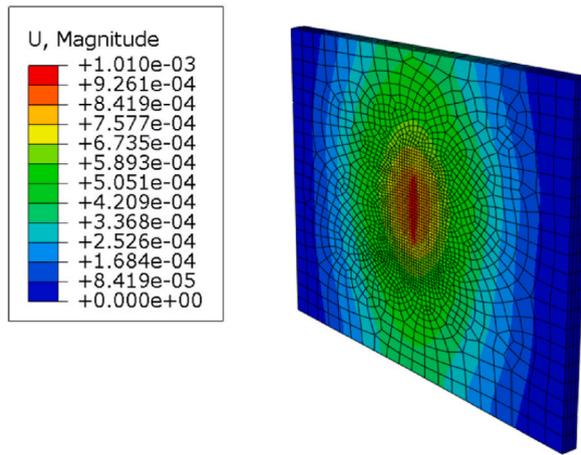
Fig. 9. The simulated deflection for case scenario 1.
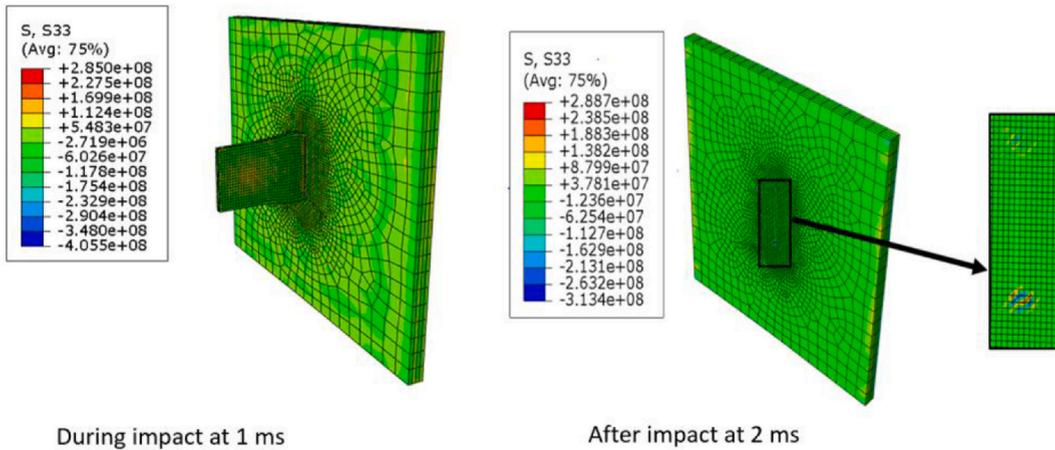
Fig. 10. the maximum stress of the simulation for case scenario 1.
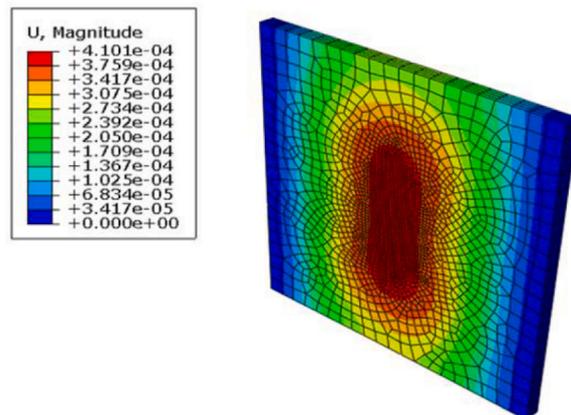
Fig. 11. The simulated deflection for case scenario 2.

3.3.3. Sensitivity results

The deflection, maximum stresses, and strain energy of all 8 case scenarios examined in this study were used as the basis for the sensitivity analysis. Fig. 16 shows the order of the increase in plastic deformation of the various case scenarios, while Table 18 shows
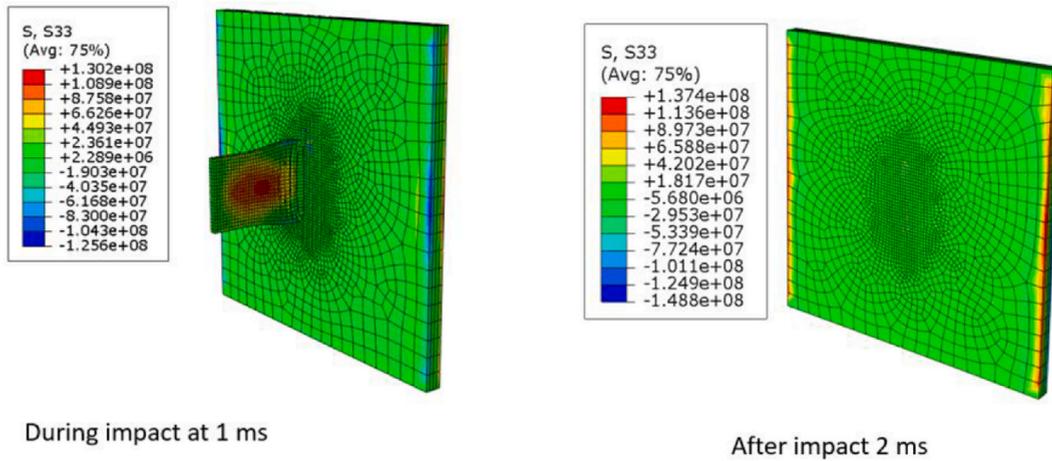
Fig. 12. the maximum stress of the simulation for case scenario 2.

Table 16
The MI methodology for case scenario 1.

Breadth (mm)	Moment of Inertia (M^4)	Deflection (mm)	Static Stress (MPa)
22	2.3×10^{-10}	0.255	9.1
21	2.2×10^{-10}	0.267	9.5
20	2.1×10^{-10}	0.281	9.8
19	1.9×10^{-10}	0.295	10
18	1.8×10^{-10}	0.312	12
17	1.7×10^{-10}	0.33	13
16	1.6×10^{-10}	0.351	14
15	1.5×10^{-10}	0.374	15
14	1.4×10^{-10}	0.401	17
13	1.3×10^{-10}	0.432	18
12	1.1×10^{-10}	0.468	20
11	1×10^{-10}	0.51	21
10	1×10^{-10}	0.561	22
9	9.4×10^{-11}	0.623	25
8	8×10^{-11}	0.701	28
7	7×10^{-11}	0.801	30
6	6×10^{-11}	0.935	30
5	5.2×10^{-11}	1.11	40
4	4×10^{-11}	1.4	50
3	3×10^{-11}	1.87	60
2	2×10^{-11}	2.8	90
1	1×10^{-11}	5.61	200

the deflection of the case scenarios upon impact. Table 19 presents the maximum stress analysis after impact for the case scenarios, and Table 20 presents the strain energy for each of the eight case scenarios. The intention was to analyze the deflection of the FC in order to establish the FB's maximum deflection or penetration depth. It can be shown that none of the impacts pierced the FCs in any of the assessments and outcomes of the case scenarios. The MI methodology and the calculation of the maximum stress and deflection correlated well. The simulated strain energy graph and MI methodology exhibit a similar behavior for the strain energy of the case scenarios. The case scenarios impacted with the aluminium FB produced more strain energy and more deformation with a stabilized dynamic penetration effect in contrast to the case scenarios impacted with PEEK, which took longer to stabilize their penetration effect but showed less FC deflection., The FB that would deform the FC more was also determined by the kinetic energy of both FBs.

4. Discussion and findings

4.1. Discussion

The number of elements on the FC's borders and the mesh size at the impact zone both significantly affected the simulation's outcomes. To achieve good correlation, it was found that the thinner FC plate dimensions needed a coarse mesh size at the impact zone and fewer elements on the sides of the edges, whereas the thicker FC plate dimensions needed a finer mesh size at the impact zone and more elements on the sides of the edges. Fundamentally, the thickness of the FC decides whether the FB impact will enter the FC or

Table 17
The MI methodology for Case scenario 2.

Breadth (mm)	Moment of Inertia (M^4)	Deflection (mm)	Static Stress (MPa)
22	2.3×10^{-10}	0.0911	3
21	2.2×10^{-10}	0.0977	3.2
20	2.1×10^{-10}	0.1	3.5
19	1.9×10^{-10}	0.105	4
18	1.8×10^{-10}	0.11	4
17	1.7×10^{-10}	0.111	4.1
16	1.6×10^{-10}	0.125	4.2
15	1.5×10^{-10}	0.134	4.8
14	1.4×10^{-10}	0.143	5
13	1.3×10^{-10}	0.154	5
12	1.1×10^{-10}	0.167	6
11	1×10^{-10}	0.182	6
10	1×10^{-10}	0.2	7
9	9.4×10^{-11}	0.223	7
8	8×10^{-11}	0.25	8
7	7×10^{-11}	0.286	10
6	6×10^{-11}	0.334	10
5	5.2×10^{-11}	0.401	13
4	4×10^{-11}	0.501	20
3	3×10^{-11}	0.668	20
2	2×10^{-11}	1	30
1	1×10^{-11}	2	70
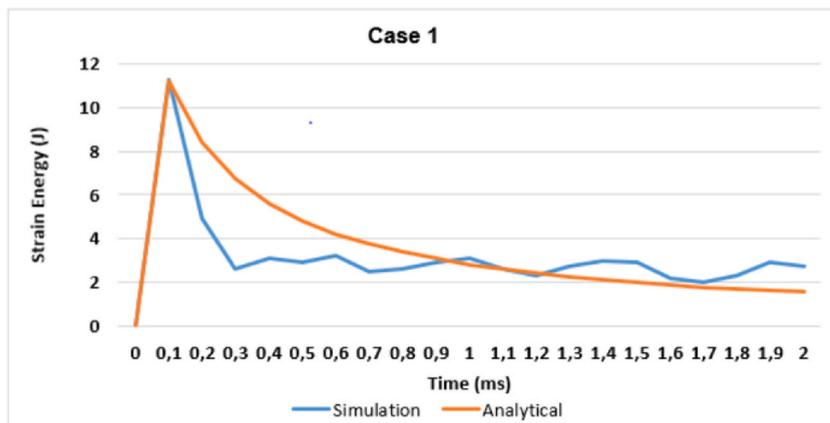
Fig. 13. Strain energy of case scenario 1.
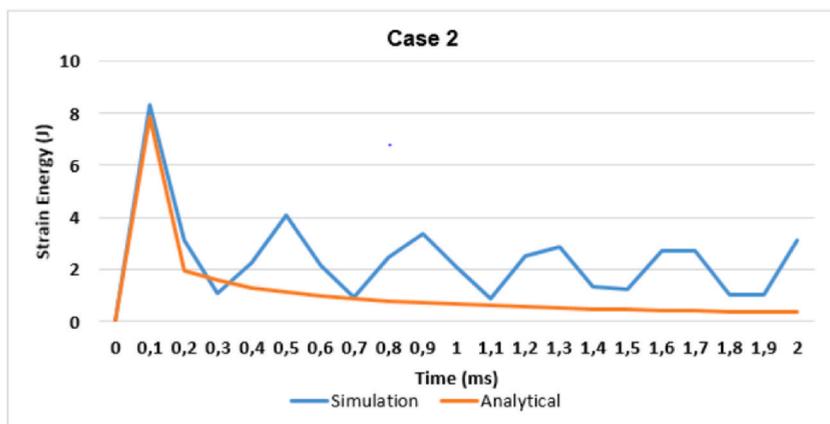
Fig. 14. Strain energy of case scenario 2.
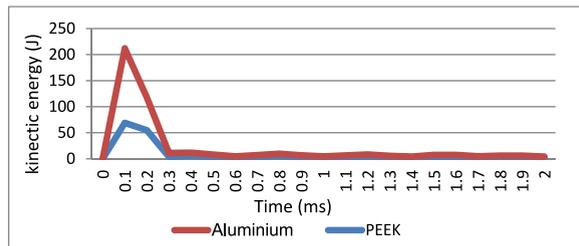
Fig. 15. Kinetic energy of the FBs.
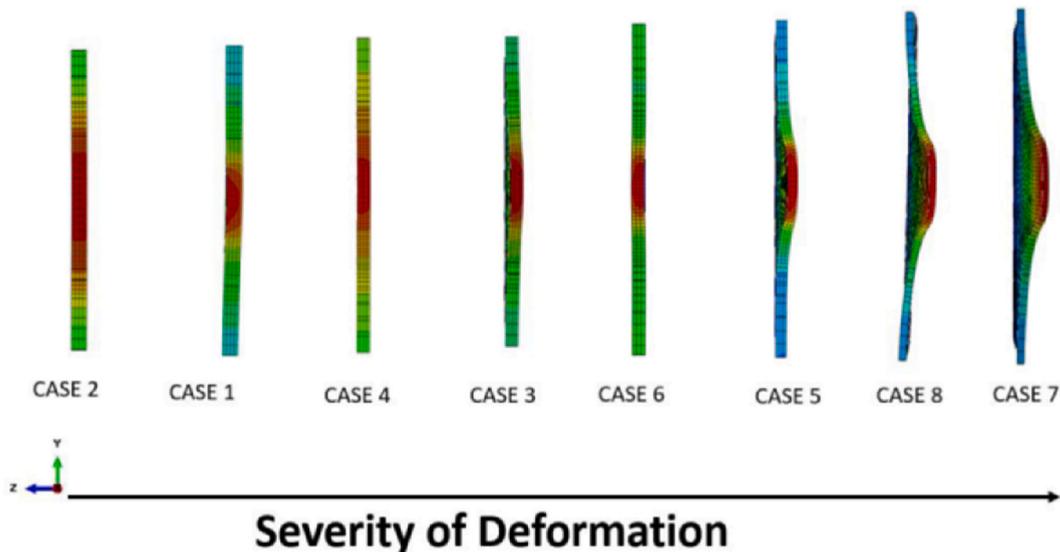
Fig. 16. Order of severity of deformation of the 8 case scenarios.

Table 18
Deflection sensitivity of the 8 case scenarios (CS).

Deflection (mm)				
CS	FC thickness and FB material	Simulation	Analytical	% Difference
1	5 mm FC and Aluminium FB	1.01	1.11	9
2	5 mm FC and PEEK FB	0.401	0.041	2
3	4 mm FC and Aluminium FB	2.79	2.74	1.5
4	4 mm FC and PEEK FB	0.578	0.559	3
5	3 mm FC and Aluminium FB	4.45	4.33	3
6	3 mm FC and PEEK FB	0.775	0.773	0.25
7	2 mm FC and Aluminium FB	9.64	9.74	1
8	2 mm FC and PEEK FB	4.7	4.47	5

generate a deflection that will harm nearby wires or sensors. It was found that the deflection sharply increases after the FB to FC ratio reaches 1:1.5, at which point the deflection exceeds the thickness of the FC. A deflection ratio of this kind can damage the sensors or cables close to the FC. The impact is significantly influenced by the kinetic friction between the projectiles and the FC. As a result, none of the FB that pierced the FC showed signs of the friction's impact resistance; instead, some collisions merely caused the FC to swell. Cases 2, 4, and 6 all had modest deflection of the 5 mm, 4 mm, and 3 mm FCs due to the PEEK FB impact. All three of the cases were found to be eligible for blade containment since the three deflections were so slight. The deflection for case 8, a 2 mm FC that was struck by a PEEK FB, was roughly twice as thick as the FC, preventing the FB from penetrating the FC. However, it was decided that it was not suitable for blade confinement since it would cause additional damage to the aircraft engine.

In cases 1 and 3, the impact of the aluminum FB caused greater damage to the 5 mm and 4 mm FCs, despite the fact that the deflection was less than the thicknesses of the FCs. This suggests that the FCs would confine the FB without causing any additional damage. However, in cases 5 and 7, which involved FCs with thicknesses of 3 mm and 2 mm, respectively, the aluminium FB severely damaged those FCs as a result of the extremely high deflections that it was subjected to. This suggests that taking into account the 3 mm

Table 19
Maximum stress sensitivity of the 8 case scenarios (CS).

Maximum Stress (MPa)				
CS	FC thickness and FB material	Simulation	Analytical	% Difference
1	5 mm FC and Aluminium FB	288	304	5
2	5 mm FC and PEEK FB	137	148	7
3	4 mm FC and Aluminium FB	491	462	6
4	4 mm FC and PEEK FB	195	188.5	3.5
5	3 mm FC and Aluminium FB	669	632	6
6	3 mm FC and PEEK FB	357.5	389.9	8
7	2 mm FC and Aluminium FB	1798	1619	9
8	2 mm FC and PEEK FB	679	632	7

Table 20
Strain energy of the 8 case scenarios.

Strain Energy (J)				
CS	FC thickness and FB material	Simulation	Analytical	% Difference
1	5 mm FC and Aluminium FB	11.4	11.2	2
2	5 mm FC and PEEK FB	8.2	7.85	4
3	4 mm FC and Aluminium FB	15.58	16.5	6
4	4 mm FC and PEEK FB	5.4	15.1	6
5	3 mm FC and Aluminium FB	15.3	15.6	2
6	3 mm FC and PEEK FB	8.85	9.08	2.5
7	2 mm FC and Aluminium FB	10	10.5	5
8	2 mm FC and PEEK FB	4.3	4.09	5

and 2 mm FCs would be risky. The aircraft would malfunction from this kind of damage, and the engine would probably shut off. The visible dents indicate that the cables and sensors may have been damaged. The FB containment simulation was modeled utilizing the J-C simulation methodology. The findings showed that the Johnson-Cook model's plasticity behavior works mediocrely well for blade containment issues. This was seen in the behavior of the PEEK and aluminum FBs as they affected the varied thicknesses of aluminum FCs in the numerical simulation.

When the aluminium FB struck the FCs, these FCs underwent significant plastic deformation, but no penetration occurred in any simulation. The impacted FCs did not undergo any appreciable plastic deformation in relation to the PEEK FB. The following observations from several cases are provided:

Cases 1 and 2 include the 5 mm casing being struck by aluminium and PEEK FBs, respectively. The results of the MI methodology are consistent with the minor deflection that was seen on the FC from the impacts of these FBs. Both FBs were appropriate in this situation because none of them managed to breach the 5 mm FC. Additionally, the deflection on both cases is substantially smaller than the actual FC thicknesses. The deflections of the PEEK and aluminum FBs were, respectively, 0.41 mm and 1.01 mm. From these findings, it was clear that the PEEK FB was better suited due to its contribution to lowering the aircraft's overall weight, improving fuel efficiency, and resulting cost reduction. The PEEK blade does not harm the case as severely as the aluminium blade, according to the simulation stress findings of the impacts of both blades. Regarding cases 3 and 4, the 4 mm FC that was struck by the aforementioned FBs deflected by 2.7 mm for the aluminium FB and by 0.578 mm for the PEEK FB. But neither of the FBs managed to enter the FC. The cables and sensors may be compressed by the FC's deflection brought on by the aluminum FB. This could lead to the sensors gradually failing and the wires connecting the engine and control system malfunctioning, which could lead to an aircraft failure.

Cases 5 and 6, which had 3 mm FCs, had an aluminum FB impact deflection of 4.45 mm but no penetration. The attached sensors would suffer immediate damage even if there was no penetration since the impact of the FB on the FC may create sharp edges that could damage the aircraft's body structure. On the other hand, the PEEK FB's impact on the FC resulted in a modest 0.56 mm deflection. Results from cases 7 and 8 showed that a 2 mm FC that had been struck by both an aluminum and a PEEK FBs deflected by 9.13 mm and 4.7 mm, respectively. In this instance, neither of the blades broke through the FC. The sensors and cables would suffer severe damage since the impact deflections of the FBs are far greater than the thickness of the casing. This demonstrated that the post-yield deformation of the 2 mm FC had occurred, which is outside the scope of the current investigation and is not described here. The 2 mm FC shouldn't be employed, according to the judgment drawn in this case after observation.

The MI methodology's findings were consistent with the deflections of all the FCs. To validate the MI methodology, the stress simulation of the analysis on the various casing thicknesses was performed. If the stress and deflection percentage errors are both larger than 10 %, it might be wise to conduct experiments to verify the findings. Both the projectile and the target bend when they collide, yet the mass and material characteristics are unaltered. These shape alterations have an impact on the MI because of the plastic deformation. The proposed MI methodology accurately validated the generated numerical model, with good correlations between all eight simulated deflections and maximum stresses in both methods. The suggested moment of inertia approach takes into account the deformation that occurs between the projectile and target during impact, which modifies the MI. Studies in the literature have demonstrated that after an impact, the shapes of two colliding bodies change. As a result, the FC and FB's moment of inertia were

changed for this investigation.

On the four various thicknesses of the casings, the strain energy exhibited dynamic behavior. According to the examination of the FC strain energy, all of the graphs have a single plateau, which is then followed by a slow decline and a stable region. According to Olsson, Donadon, and Falzon [33], an impactor will react energetically differently to projectiles of differing masses. The impact of PEEK and aluminum FBs in this investigation showed that a tiny mass projectile will not have enough time to deflect and will behave transversely from the impactor. Despite sharing the same properties, the strain energy graphs stabilized at different values. As a result, it was shown that the dynamic effects on FCs by the PEEK FB are unstable and take some time to stabilize. The time at which the deformation occurs is indicated by the plateau. After then, the strain energy steadily drops and stabilizes, leading to a no penetration event at 255 m/s in velocity. The strain energy graphs produced by the numerical model and those produced by the MI methodology, both demonstrated the same pattern and a very strong correlation, it is crucial to note at this point.

Findings showed that the high energy of both the aluminum and the PEEK FBs was 0.3 ms (ms), when comparing the kinetic energy findings of the two types of FBs. The plateau seen in the graph of the aluminum FB, however, is larger than that of the PEEK FB. If the speed were raised, the aluminum FB's material qualities would cause a distortion that would seriously damage the FC or enter the FC. Even if the speed is increased, the PEEK blade is less likely to penetrate since its kinetic energy is roughly one-fourth that of the aluminum FB. Instead, it might cause the blade to shatter or the FC to deflect more. The numerical model was unable to account for all the incidences that occurred during the experiments, according to Sharma et al. [34], who discussed the noticeable error discrepancy between the experimental and numerical assessments. Because the MI methodology in this study is unable to account for the temperature-related incidents that happened in the numerical model, it may be concluded that there is an error difference between the numerical model and that methodology.

4.2. Findings

1. No penetration was seen in any of the cases, regardless of the FB material or FC thickness; nonetheless, the amount of deformation decreased as the FC thickness increased.
2. The strain energy, maximum stress, and deflection sensitivity analysis tables all displayed the same deformation pattern.
3. Excessive plasticity was present in Cases 8, 7, 5, and 3, in that sequence.
4. Cases 2, 1, 4, and 6, in the order given, deform within the elastic zone.
5. The outcomes showed that the model's plasticity behavior, as predicted by Johnson-Cook, is effective for solving FB containment issues.
6. The proposed MI methodology accurately validated the constructed numerical model, and all of the deflection and maximum stresses for the eight simulated cases closely correlated.

5. Conclusions

A new methodology MI approach was developed to account for a projectile's ability to instantly change shape. The simulation model and the MI methodology have a high correlation. Prior research on ballistic test experiments has proved to be expensive. Hence, the MI methodology has shown to be a practical and affordable way to validate the numerical model. The findings led to the following.

- The MI of the case was influenced by the FB's shape, and it influences how resistant it is to deflection.
- There was a correlation between the simulation (conducted using ABAQUS/Explicit 2017) and the MI methodology.
- The MI methodology is appropriate for ballistic collisions

Based on these findings lead it is concluded that PEEK can be utilized to make FBs because of the material's dependability and potential to reduce the risk of non-containment problems. In addition, PEEK material is appropriate for a 2 mm FB with a 5 mm or 4 mm FC. Another benefit is that manufacturing a PEEK FB only requires two days, compared to seven days for an aluminum FB. The order of rank for a different range to choose the best FC would be Case 2, 1, 4, 3, 6, 5, and 7. Using the MI methodology, additional research on the impact of various projectile shapes can be conducted.

Data availability statement

Data associated with this study has been deposited into Tshwane University of Technology library - Pretoria Campus.

Additional information

No additional information is available for this paper.

CRediT authorship contribution statement

Shade Rouxzeta VAN Der Merwe: Writing – review & editing, Writing – original draft, Visualization, Validation, Supervision, Software, Resources, Project administration, Methodology, Investigation, Funding acquisition, Formal analysis, Data curation, Conceptualization, Writing – review & editing, Writing – original draft, Visualization, Validation, Supervision, Software, Resources,

Project administration, Methodology, Investigation, Funding acquisition, Formal analysis, Data curation, Conceptualization. **Dawood Ahmed Desai:** Writing – original draft, Visualization, Validation, Supervision, Software, Resources, Project administration, Methodology, Investigation, Funding acquisition, Formal analysis, Data curation, Conceptualization. **Glen Campbell Snedden:** Writing – original draft, Visualization, Validation, Supervision, Software, Resources, Project administration, Methodology, Investigation, Funding acquisition, Formal analysis, Data curation, Conceptualization. **Daniel Ogochukwu Okanigbe:** Writing – review & editing.

Declaration of competing interest

Acknowledgements

References

[1] E. Silveira, G. Atxaga, A.M. Irisarri, Failure analysis of two sets of aircraft blades, Eng. Fail. Anal. 17 (3) (2010) 641–647.
[2] A.C. Kemp, J. Dalal, U. Tassawar, C.T. Lu, Safety analysis of uncontained engine failure-Southwest Airlines flight 1380, International Journal of Crisis Management 11 (1) (2021) 13–23.
[3] A. Kanso, L. Grassmuck, A Crisis in the Air: Analyzing public relations at southwest airlines to restore public trust, in: Competition Forum (Vol. 18, No. 1/2, Pp. 148-156), American Society for Competitiveness, 2020.
[4] A.N. Kane, A.S. Jadhav, S. Sahamate, V. Kokare, K.B. Jadhav, Review of aircraft crash reports and engine pod location, in: 2021 IEEE Pune Section International Conference (PuneCon), IEEE, 2021, December, pp. 1–9.
[5] H.J. Xuan, R.R. Wu, Aeroengine turbine blade containment tests using high-speed rotor spin testing facility, Aero. Sci. Technol. 10 (6) (2006) 501–508.
[6] Z. He, H. Xuan, C. Bai, Y. Hu, P. Cong, H. Bai, W. Hong, Containment tests and analysis of soft wall casing fabricated by wrapping Kevlar fabric around thin metal ring, Aero. Sci. Technol. 61 (2017) 35–44.
[7] B. Yang, Blade containment evaluation of civil aircraft engines, Chin. J. Aeronaut. 26 (1) (2013) 9–16.
[8] Q. He, H.J. Xuan, L.F. Liao, W.R. Hong, R.R. Wu, Simulation methodology development for rotating blade containment analysis, J. Zhejiang Univ. - Sci. 13 (2012) 239–259.
[9] K.S. Carney, J.M. Pereira, D.M. Revilock, P. Matheny, Jet engine fan blade containment using an alternate geometry, Int. J. Impact Eng. 36 (5) (2009) 720–728.
[10] B. Horton, J. Bayandor, Numerical investigation of fan-blade out using meso-scale composite modeling, in: 30th Congress of the International Council of the Aeronautical Sciences, ICAS, 2016, pp. 1–8.
[11] W. Li, M.F. Goodchild, R. Church, An efficient measure of compactness for two-dimensional shapes and its application in regionalization problems, Int. J. Geogr. Inf. Sci. 27 (6) (2013) 1227–1250.
[12] S. Selepe, Containments Test Report, CSIR, Aeronautical Systems, 2018.
[13] J.M. Gere, B.J. Goodno, Mechanics of Materials, Cengage learning, 2012.
[14] N. Cosme, D. Chevrolet, J. Bonini, B. Peseux, P. Cartraud, Prediction of transient engine loads and damage due to hollow fan blade-off, Revue Européenne des Eléments 11 (5) (2002) 651–666.
[15] P. Sharma, P. Chandel, V. Bhardwaj, M. Singh, P. Mahajan, Ballistic impact response of high strength aluminium alloy 2014-T652 subjected to rigid and deformable projectiles, Thin-Walled Struct. 126 (2018) 205–219.
[16] S.I. Moon, C.H. Kim, J.C. Koo, J.B. Choi, Y.J. Kim, Y.J. Kim, Simplified static analysis for shock behavior evaluation of thin glass plates, Solid State Phenom. 110 (2005) 263–270.
[17] Q. He, Z. Xie, H. Xuan, L. Liu, W. Hong, Multi-blade effects on aero-engine blade containment, Aero. Sci. Technol. 49 (2016) 101–111.
[18] J.F. Chinella, B. Pothier, M.G. Wells, Processing, Mechanical Properties, and Ballistic Impact Effects of Austempered Ductile Iron, Army Research Lab Aberdeen Proving Ground Md, 1998.
[19] C.A. Calder, W. Goldsmith, Plastic deformation and perforation of thin plates resulting from projectile impact, Int. J. Solid Struct. 7 (7) (1971) 863–881.
[20] H. Amarchinta, Uncertainty Quantification of Residual Stresses Induced by Laser Peening Simulation, 2010.
[21] Q. He, H.J. Xuan, L.F. Liao, W.R. Hong, R.R. Wu, Simulation methodology development for rotating blade containment analysis, J. Zhejiang Univ. - Sci. 13 (2012) 239–259.
[22] A. Hor, F. Morel, J.L. Lebrun, G. Germain, Modelling, identification and application of phenomenological constitutive laws over a large strain rate and temperature range, Mech. Mater. 64 (2013) 91–110.
[23] M. Kumar, U. Deep, P.M. Dixt, Simulation and analysis of ballistic impact using continuum damage mechanics (CDM) model, Procedia Eng. 173 (2017) 190–197.
[24] K. Jamison, S. Sneddon, G. Turner, Developing a Ram-Air Turbine (RAT) Power Supply System for a High-Speed, CSIR: Aeronautical Systems, 2018.
[25] I.S. Boldyrev, I.A. Shchurov, A.V. Nikonov, Numerical simulation of the aluminum 6061-T6 cutting and the effect of the constitutive material model and failure criteria on cutting forces' prediction, Procedia Eng. 150 (2016) 866–870.
[26] D. Garcia-Gonzalez, A. Rusinek, T. Jankowiak, A. Arias, Mechanical impact behavior of polyether–ether–ketone (PEEK), Compos. Struct. 124 (2015) 88–99.
[27] Q. He, H.J. Xuan, L.F. Liao, W.R. Hong, R.R. Wu, Simulation methodology development for rotating blade containment analysis, J. Zhejiang Univ. - Sci. 13 (2012) 239–259.
[28] DASSAULT. 6.14. Continuum elements. In Guide, A.a.U.S. (Ed.), SIMULIA. Online.
[29] D.A. Desai, Prediction and Reduction of Low-Frequency Vibro-Acoustic Transmission through Automotive Door Mounts, 2010.
[30] A.U.S. Manual, Dassault Systémes Simulia Corp, providence, Rhode Island, USA, 2012.
[31] N. Behary, Micro Gas Turbine Parameterised Shaft Design, 2015.
[32] K. Koenig, N.D. Mitchell, T.E. Hannigan, J.K. Clutter, The influence of moment of inertia on baseball/softball bat swing speed, Sports Eng. 7 (2004) 105–117.
[33] R. Olsson, M.V. Donadon, B.G. Falzon, Delamination threshold load for dynamic impact on plates, Int. J. Solid Struct. 43 (10) (2006) 3124–3141.
[34] A. Sharma, R. Mishra, S. Jain, S.S. Padhee, P.K. Agnihotri, Deformation behavior of single and multi-layered materials under impact loading, Thin-Walled Struct. 126 (2018) 193–204.